Characterization of Cu(II)-reconstituted ACC Oxidase using experimental and theoretical approaches

Nadia El Bakkali-Tahéri, Sybille Tachon, Maylis Orio, Sylvain Bertaina, Marlène Martinho, Viviane Robert, Marius Réglier, Thierry Tron, Pierre Dorlet, A. Jalila Simaan

Characterization of Cu(II)-reconstituted ACC Oxidase using experimental and theoretical approaches

Nadia El Bakkali-Tahéri,[a] Sybille Tachon,[a] Maylis Orio,[a] Sylvain Bertaina,[c] Marlène Martinho,[d] Viviane Robert,[a] Marius Réglier,[a] Thierry Tron,[a] Pierre Dorlet,[b] A. Jalila Simaan[a*]

[a] Aix Marseille Univ, CNRS, Centrale Marseille, iSm2, Marseille, France

[b] Institute for Integrative Biology of the Cell (I2BC), CNRS, CEA, Univ. Paris-Sud, Université Paris-Saclay, 91191 Gif-sur-Yvette Cedex, France

[c] Aix Marseille Univ, CNRS, IM2NP, Marseille, France

[d] Aix Marseille Univ, CNRS, BIP, Marseille, France

✉ A. Jalila Simaan, ☎+33 491289151; fax: +33 491288440, jalila.simaan@univ-amu.fr

Abbreviations: ACC: 1-aminocyclopropane-1-carboxylic acid; ACCO: 1-aminocyclopropane-1-carboxylic acid oxidase; EDTA: ethylenediaminetetraacetic acid, DTT: dithiothreitol or DL-Thréo-1,4-dimercapto-2,3-butanediol, HEPES: 2-[4-(2-hydroxyethyl)piperazin-1-yl]ethanesulfonic acid, MES: 2-(N-morpholino)ethanesulfonic acid, Tris: 2-Amino-2-hydroxymethyl-propane-1,3-diol, EPR: Electron Paramagnetic Resonance; ESEEM: Electron Spin Echo Envelope Modulation; DFT: Density Functional Theory, CD : Circular Dichroism

Abstract

1-Aminocyclopropane-1-carboxylic acid oxidase (ACCO) is a non heme iron(II) containing enzyme that catalyzes the final step of the ethylene biosynthesis in plants. The iron(II) ion is bound in a facial triad composed of two histidines and one aspartate (H177, D179 and H234). Several active site variants were generated to provide alternate binding motifs and the enzymes were reconstituted with copper(II). Continuous wave (*cw*) and pulsed Electron Paramagnetic Resonance (EPR) spectroscopies as well as Density Functional Theory (DFT) calculations were performed and models for the copper(II) binding sites were deduced. In all investigated enzymes, the copper ion is equatorially coordinated by the two histidine residues (H177 and H234) and probably two water molecules. The copper-containing enzymes are inactive, even when hydrogen peroxide is used in peroxide shunt approach. EPR experiments and DFT calculations were undertaken to investigate substrate's (ACC) binding on the copper ion and the results were used to rationalize the lack of copper-mediated activity.

Keywords:

Ethylene, ACC Oxidase, copper, Electron Paramagnetic Resonance, Density Functional Theory calculations

Introduction

Ethylene, the simplest olefin, is a hormone essential for many aspects of plant life including root development, germination, senescence, fruit ripening and defense mechanisms [1]. In 1979, Adams and Yang have reported that ethylene is directly biosynthesized from 1-aminocyclopropane-1-carboxylic acid (ACC), a metabolite of methionine [2]. 1-aminocyclopropane-1-carboxylic acid oxidase (ACCO) is a non heme iron(II) containing enzyme that catalyzes the final step of ethylene biosynthesis. In the presence of ascorbic acid, ferrous ions and dioxygen ACCO produces ethylene, cyanhydric acid and carbon dioxide (arising from cyanoformate) (Scheme 1) [3-5]. In addition, ACCO requires the presence of carbon dioxide (or bicarbonate ions) for activity [6,7].

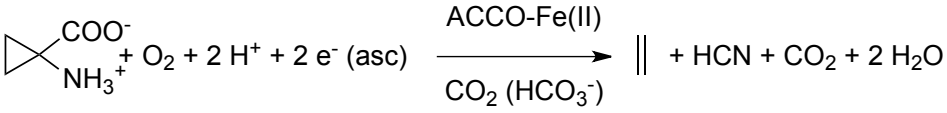

Scheme 1. Reaction catalyzed by ACCO

The structure of ACCO from *Petunia hybrida* has been solved and reveals a core composed of β-strands folded into a distorted jelly-roll motif also called Double Strand β-Helix (DSBH) fold [8]. The iron ion is ligated to the side chains of two histidines (H177 and H234) and one aspartate (D179) in a classical 2 histidines - 1 carboxylate facial triad (Figure 1). A buffer anion (sulfate or phosphate) is also bound to the iron ion. Finally, although active as a monomer, the protein crystallizes as a tetramer and a glutamate residue (E80) from an adjacent monomer is located at *ca*. 3 Å from the metal. This form probably does not correspond to an active conformation and spectroscopic studies have led to a model of the resting state in which the iron(II) is in octahedral geometry with three water molecules bound to complete the coordination sphere [9]. The iron center therefore exhibits three available coordination sites for exogenous ligand coordination and reactivity. On the basis of structure

and sequence, ACCO is related to the 2-oxoglutarate dependent dioxygenases, an extended family of Fe(II)-containing enzymes that use 2-oxoglutarate as a cofactor to perform the oxidation of various substrates [10-12].

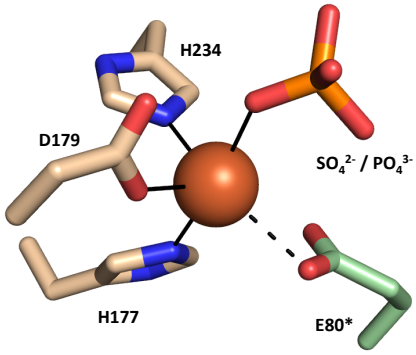

Figure 1. Structure of the active site of ACCO-Fe(II) (pdb 1WA6)

The conversion of ACC into ethylene by ACCO proceeds *via* the formation of an aminyl radical and a sequential radical mechanism [13]. Thanks to extensive EPR and ENDOR studies of the EPR-active Fe(II)-NO complex of ACCO, it has been proposed that ACC binds to the ACCOFe^{II} resting-state allowing O_2 binding to yield a putative ACCOFe^{III}ACC-superoxo intermediate [14],[15]. The ACC is found coordinated in a bidentate fashion *via* the nitrogen of the amine and an oxygen of the carboxylate group. Rocklin *et al*. have proposed that this Fe^{III}-superoxo complex is reduced by an electron from ascorbate to yield an ACCOFe^{III}ACC-peroxo complex (or hydroperoxo upon proton transfer) that would be the first oxidizing intermediate [16]. Alternatively, using solvent isotope effects and kinetic isotope effects (^{18}O), the group of Klinman has proposed that a second reduction occurs to yield an Fe^{IV}=O species which would act as the reactive intermediate in substrate oxidation [17]. Direct experimental detection of reactive intermediates is nevertheless lacking and the exact iron-centered oxidizing intermediates are still the object of debates [16,17].

Bio-inspired model complexes have provided valuable structural and mechanistic information on metal-containing enzymes. In the case of ACCO, two Fe(II)-ACC complexes that are

structural models for the enzyme-substrate complex were very recently reported (Scheme 2) [18],[19]. Those complexes feature the bidentate coordination of ACC on the metal center as proposed for the enzyme. In particular, the trispyrazolylborate-containing [$Tp^{Me,Ph}$FeACC] complex was the first known ACCO model complex that reacts with O_2 to produce ethylene. In addition, reaction with H_2O_2 led to fast ethylene evolution with 65% yield [19].

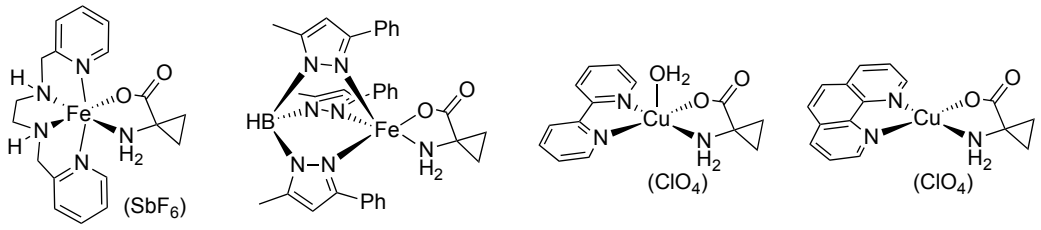

Scheme 2. Examples of metal-ACC bioinspired model complexes of ACCO.

Several years ago, we have reported on a series of structurally characterized Cu(II)-ACC complexes using aminopyridine-type ligands in which ACC is coordinated on the Cu(II) ion in a bidentate manner [20],[21],[22]. These complexes are able to oxidize the bound ACC into ethylene in the presence of hydrogen peroxide. In addition, copper-based complexes are also able to oxidize other aminoacid substrates [23,24]. The product distribution obtained using those substrate analogs suggests that these complexes follow substrate oxidation pathways sharing similarities with the enzymatic ones, although the oxidizing intermediates are probably different from those involved in the iron(II)-dependent enzyme. In addition, structural and functional copper-containing models of 2-oxoglutarate dependent dioxygenases have also been reported [25,26].

We were therefore very interested in characterizing and evaluating the properties of copper-reconstituted ACCO. Considering the coordination motifs observed in natural systems or used in model chemistry [27,28], site-directed ACCO variants were generated to provide alternate coordination patterns: the aspartate was replaced either by an alanine (D179A to provide a 2-

His binding site) or a histidine (D179H, 3-His). In an attempt to modulate the geometry and flexibility around the metal ion, we also replaced the aspartate by a glutamate (D179E, 2-His, 1-Glu). In the present work, the catalytic potential of ACCO-Cu(II) enzymes for ethylene production including through peroxide shunt reaction was explored. The impact of variations in the first coordination sphere on the geometric and electronic metal center structure were evaluated spectroscopically and correlated with DFT studies of the metal binding site.

Materials and methods

All chemicals were purchased from Sigma-Aldrich and used without further purification except 1-aminocyclopropane carboxylic acid (ACC) that was purchased from ACROS Organics.

Construction of the site-directed variants

The plasmid containing the gene encoding for the ACCO from *Petunia hybrida* (Q08506) was donated by the group of C. Schofield from Oxford University (United Kingdom) [8]. Point mutations were introduced by PCR, using the QuikChange II XL Site-Directed Mutagenesis kit (stratagene). The primers used (Table 1) were designed using the QuikChange Primer Design tool available online (http://www.genomics.agilent.com/primerDesignProgram.jsp). PCRs were run for 18 cycles of 50 s at 95°C and 50 s at 60°C, followed by 6 min at 68°C. The resulting mutant plasmids were verified by DNA sequencing (Beckman Coulter Genomics).

Table 1. Primers used for the construction of the variants

Mutation	Forward primer sequence[a]
D179H	5'-gactacgtgcccacacacacgctggtg-3'
D179A	5'-ctacgtgcccacacagcggctggtggcataatcc-3'
D179E	5'-ctacgtgcccacacagaagctggtggc-3'

[a] the reverse primers used were the complements of the forward primers

Overexpression and purification of recombinant enzymes

The recombinant enzymes were expressed in *Escherichia coli* strain BL21(DE3) following the already described procedure [8,29]. Cells were grown in flasks at 37°C (200 rpm) in 2 L Terrific Broth media containing 15 µg/mL of tetracycline to an $OD_{600} \approx 1$. The temperature was then shifted to 28°C and the culture was grown for another 40 minutes before protein expression was induced by the addition of 0.5 mM isopropyl-β-D-thiogalactopyranoside. After 3 hours of induction at 28°C (200 rpm), cells were harvested by centrifugation (5000g, 4°C, 15 min using a BECKMAN JA 2550) and frozen at -20°C. Purification steps were performed at 4°C. Thawed cell pellets were re-suspended in buffer containing 25 mM HEPES at pH = 8.0, 10% glycerol, 3 mM EDTA, 5 mM DTT, 1 mM benzamidine, 10µM leupeptine, 1µg/mL pepstatine and 0.8 mM pefablock. Lysis was performed using a FRENCH® press (Thermo Scientific). Cell debris were eliminated by centrifugation (1h at 18000 rpm; BECKMAN JA 2550). The supernatant was loaded on a Q-Sepharose resin (GE Healthcare) equilibrated with buffer A (HEPES 25 mM pH 8.0, 10 % glycerol, 3 mM EDTA, 1mM benzamidine, 5mM DTT) and eluted with increasing concentrations of buffer B (A+ 1 M of NaCl). Fractions containing ACCO were dialyzed against 25 mM HEPES pH=7.2 containing 10% glycerol and stored at -20°C at concentrations ranging from 5-10 mg/mL.

Circular Dichroism

Far UV Circular dichroism spectra were measured using a JASCO J-815 spectrometer equipped with Peltier cell holder PTC-423 to maintain the temperature at 20.0±0.2 °C. Measurements were performed from 250 to 190 nm using 0.1 nm step size. The proteins were placed in a 0.1 cm path length quartz cuvette at concentrations of 0.1 or 0.2 mg/mL. Buffer used was either 10 mM phosphate set at pH=7.5 or 10 mM Tris-H_2SO_4 set at pH=7.2. $CuSO_4.5H_2O$ was added from concentrated stock solutions in water.

Activity assays

Standard assay conditions were performed at 29°C in 1.7 mL hermetically sealed vials. The total assay volume was 200 μL containing: 25 mM HEPES buffer at pH=7.2 with 10% glycerol, 4 μg of enzyme, 15 mM $NaHCO_3$, 8 mM L-ascorbic acid, 80 μM $Fe(SO_4)_2(NH_4)_2.6H_2O$ and 1.25 mM ACC. After 7 minutes of reaction, 1 mL of the headspace gas was removed using a gas-tight syringe and ethylene production was quantified by Gas Chromatography. Note that the production of ethylene is found to be linear over 10 minutes, as previously reported [29]. For the determination of kinetic parameters, measurements were performed varying the concentration of one substrate while maintaining the others at the above-mentioned concentrations. Variation ranges were 0-1.75 mM for ACC, 0-12 mM for ascorbate, 0-18 mM for $NaHCO_3$ and 0-100 μM for $Fe(SO_4)_2(NH_4)_2.6H_2O$. Non-linear curve fitting to the Michaelis-Menten equation (eq. 1) were performed using GraphPad Prism 6.0 to determine apparent kinetic constants.

(eq. 1) $$v = \frac{V_{\max}.[S]}{K_M + [S]}$$

Inhibition studies

Inhibition studies were performed following the activity assay conditions mentioned above. Experiments were performed in the presence of several concentrations of $CuSO_4.5H_2O$ (ranging from 0-6 μM) and varying the concentration of Fe(II) (from 0-80 μM) while maintaining the other substrates or cofactors at their above-mentioned concentrations. Each reaction was repeated at least 3 times. Inhibition types were determined using Lineweaver-Burk representations as well as by using the method proposed by Cornish-Bowden [30]. Inhibition constant was determined using non-linear curve fitting and the set of curves was fit simultaneously. Equation 2 displaying the initial velocity was used for competitive inhibition pattern.

(eq. 2) $v = \frac{V_{max}.[Fe]}{K_M.(1+\frac{[Cu]}{K_i})+[Fe]}$, where K_i is defined as the dissociation constant for the Enzyme/Inhibitor complex;

Activity assay of copper(II)-reconstituted enzymes

Ethylene production was also assayed by replacing the iron salt by $CuSO_4.5H_2O$ and using the above-mentioned conditions and concentrations for the other cofactors / cosubstrates. In this case, 4μg of enzyme was used and the concentration of Cu was varied from 5-100 μM.

The activity was also assayed using hydrogen peroxide. In this case, ACCO enzymes were placed at concentrations of 100-200 μM in the presence of 1 equivalent of $CuSO_4.5H_2O$. 1-10 equivalents of ACC and 0, 1 or 10 equivalents of bicarbonate were added. Hydrogen peroxide (1-10 equivalents) was injected through the septum to initiate the reaction. After one hour, 1 mL of the headspace gas was removed using a gas-tight syringe and analyzed by Gas Chromatography. Control reactions were performed using identical conditions but in the absence of enzyme. In order to evaluate the effect of buffer/pH, the assays were performed

either in 25 mM MES pH 6.5, 25 mM HEPES pH 7.2, 50 mM TRIS-HCl pH 7.5 or 50 mM carbonate buffer at pH 10.

Gas chromatography

Measurements were performed on a SHIMADZU GC-2014A equipped with a PORAPAK Q 80/100 column (1/8″) and a FID detector. The following conditions were used: vector = N_2, $T_{injector}$ = 250°C, T_{oven} = 150°C, $T_{detector}$ = 250°C. Ethylene was quantified using a standard curve of ethylene (Scotty 1% ethylene in nitrogen).

Fluorescence measurements

Fluorescence measurements were performed at 20°C using a Horiba Jobin-Yvon Fluoromax-4 spectrometer. The excitation wavelength was 290 nm (1 nm excitation slit widths), and the emission wavelength was 345 nm (5 nm slit widths). Titration experiments were performed using 0.65 µM of ACCO in 50 mM Tris-HCl buffer (pH 7.2) and $Fe(SO_4)_2(NH_4)_2.6H_2O$ or $CuSO_4.5H_2O$ was then added in portions of 1–20 µL from freshly prepared concentrated stock solutions. Titration experiments were reproduced at least 3 times. Fluorescence changes were analyzed by curve fitting (GraphPad Prism 6.0b) according to equation 3 (See SI for details).

$$\text{(eq. 3)}\ \frac{I_0 - I}{I_0} = \frac{\Delta I_{max}}{I_0} * \frac{(K_d + E_T + L_T) - \sqrt{(K_d + E_T + L_T)^2 - 4E_T L_T}}{2E_T}$$

Where E_T is the enzyme concentration, L_T is the cofactor concentration, K_d is the dissociation constant and ΔI_{max} is the maximum fluorescence quenching at high cofactor concentration (infinite limit). K_d and $\Delta I_{max}/I_0$ were obtained from curve-fitting analysis.

EPR measurements and simulation

Protein samples were placed at concentrations ranging from 280-350 μM in 50 mM Tris-HCl buffer set at pH 7.2 and containing 10% glycerol. A 0.1 M stock solution of $^{63}Cu(NO_3)_2$ obtained by nitric acid treatment of isotopically pure ^{63}Cu (Eurisotop, Saclay, France) was used and the proteins were reconstituted with 0.9 equivalent of $^{63}Cu(II)$. To study the effect of substrate binding, 1-10 equivalents of ACC were added on the ACCO-Cu(II) complex. The *cw* EPR spectra were recorded at 9.4 GHz on frozen solution samples using a Bruker ELEXSYS 500 spectrometer equipped with a continuous flow He cryostat (Oxford) with lock-in detection using the 1st harmonic of the field modulation with amplitude 0.1 mT and frequency 100 kHz. The EPR spectra simulations have been performed using Matlab program package Easyspin [31]. The optimum Hamiltonian parameters have been obtained using the 2nd order perturbation then an exact diagonalization has been used for the final simulations. The homogenous linewidth was set to 0.3 mT, no strain of the hyperfine field and a reasonable strain of the g-tensor were used to simulate the width of the recorded lines. Pseudomodulation treatment of the spectra was performed to graphically extract the A_N superhyperfine coupling constants [32]. A_N constants were considered isotropic and used in the final simulation of the first-derivative spectra. The Hamiltonian used for the simulations is the following:

(eq. 4) $H = \mu_b S[g]B + S[A_{Cu}]I_{Cu} + S[A_{N1}]I_{N1} + S[A_{N2}]I_{N2} + \ nuclear\ zeeman$

Pulsed-EPR experiments were recorded on a Bruker ELEXSYS 580 spectrometer at liquid helium temperatures. The three-pulse (stimulated echo) sequence $\pi/2$-τ-$\pi/2$-T-$\pi/2$ was used with a pulse length $t_{\pi/2}$ of 12 ns. The time interval T was varied from 120 to 4812 ns using a 8 ns step. A four-step phase-cycle was used to eliminate unwanted echoes. The time domain spectra were baseline corrected, apodized with a Hamming window and zero-filled before

cosine Fourier transformation. Dead-time reconstruction of the time domain data was performed interactively by following the Mims' procedure [33]. Pulsed EPR data were processed by using routines locally written with Matlab (R2009a, The Mathworks, Inc.).

Structural models set-up

Structural models for copper(II)-containing native and mutants D179E, D179A and D179H were constructed using the X-ray crystal structure of the ACC oxidase (PDB code: 1WA6) [8]. To generate the native enzyme's model, the iron ion was substituted by a copper ion and the peptidic chains containing iron-coordinating histidine and aspartate residues were conserved. The chains were adequately truncated in N-terminal and C-terminal parts using methyl groups. The copper coordination sphere was completed by replacing the iron-coordinating phosphate/sulfate group with water molecules (either two or three). D179E, D179A and D179H mutants were generated by replacing the aspartate residue with a glutamate, an alanine or a histidine residue. The models for the native Cu(II)-ACC complex were generated by coordinating the ACC in bidendate or monodentate modes on the Cu(II) ion using different conformations and replacing one or two water molecules by the ACC. The resulting models were subjected to constrained minimization energy procedures. Only the first coordination sphere residues and the copper metal ion were geometry-optimized and the other residues were kept frozen at the position they initially occupy in the X-ray crystal structure.

DFT calculations

All theoretical calculations were performed with the ORCA program package [34]. Constrained geometry optimizations were carried out using the GGA functional BP86 [35-37] in combination with the TZV/P [38] basis set for all atoms and by taking advantage of the

resolution of the identity (RI) approximation in the Split-RI-J variant [39] with the appropriate Coulomb fitting sets [40]. Increased integration grids (Grid4 in ORCA convention) and tight SCF convergence criteria were used. Solvent effects were accounted for according to the experimental conditions. g-tensors and hyperfine coupling constants were obtained from single-point calculations using the B3LYP functional [41-44]. The EPR-II basis set was employed for the ligands while scalar relativistic effects were accounted for the metal complexes [45]. They were included with ZORA paired using the SARC def2-TZVP(-f) basis sets and the decontracted def2-TZVP/J Coulomb fitting basis sets for all atoms [46,47]. Increased integration grids (Grid4 and GridX4 in ORCA convention) and tight SCF convergence criteria were used in the calculation. The integration grids were increased to an integration accuracy of 11 (ORCA convention) for the metal center. Picture change effects were applied for the calculation of the hyperfine tensors.

Results

Production and characterization of the enzymes

The native enzyme (ACCO from *Petunia hybrida*) and its variants were produced as previously described and purified in the presence of EDTA [8]. EDTA was removed and the enzymes were stored in their *apo* forms. Metal reconstitution (iron or copper) was performed prior to the experiments.

The produced native and variant enzymes were then characterized. Physical characterization of the native and variant proteins by CD spectroscopy confirmed that no major changes in the secondary structure content occurred in any of the variant studied (see SI). Starting with the determination of the Michaelis-Menten parameters of the native enzyme in the presence of its natural iron cofactor, activities of the variant enzymes were then evaluated. Reaction rates were measured under initial velocity conditions while varying a single substrate in order to

determine the kinetic constants for two substrates of the reaction: ACC and ascorbate. Michaelis-Menten parameters were not determined for dioxygen, the concentration of which was *ca*. 240 µM (air-saturated water at 29°C). Although Fe(II) and HCO_3^- are cofactors/activators, they were treated as pseudo-substrates as already reported [48,49]. The determined apparent Michaelis-Menten parameters for the native ACCO from *Petunia hybrida* are reported in Table **2**. These parameters are similar to those previously reported for other ACCOs [48-50]. None of the D179 variants displayed measurable activity.

Table 2. Apparent kinetic constants for native Petunia ACCO. When kept constant, the concentration of the effectors were the following: ACC: 1.25 mM; HCO_3^-: 15 mM; Ascorbate: 8 mM; Fe(II): 80 µM.

	Fe(II)	ascorbate	ACC	HCO_3^-
k_{cat} (min^{-1})	5.5 ± 0.3	5.1 ± 0.5	6.1 ± 0.2	4.8 ± 0.2
K_M (mM)	0.007 ± 0.001	2.5 ± 0.4	0.16 ± 0.03	1.4 ± 0.3

Metal binding affinity

We further characterized the different enzymes by evaluating their metal-binding affinities. Binding constants of both Fe(II) and Cu(II) in the native and variant ACCO's active site were evaluated by fluorescence measurements. Intrinsic fluorescence of proteins, mainly of tryptophan residues, is a powerful tool to monitor metal cofactor binding to a protein [51,52]. The mechanism of fluorescence quenching upon metal binding has mainly been described as a long-range energy transfer to an absorption band produced by the metal-protein complex [53,54]. We have previously successfully applied this technique to determine the binding affinity of Fe(II) to tomato ACCO in the presence of several combinations of substrates / cofactors [29]. Our ACCO from Petunia has three tryptophan residues and the intrinsic fluorescence of the native and variant enzymes is characterized by an emission band centered

at 345 nm for an excitation wavelength of 290 nm. This emission is significantly quenched upon Fe(II) and Cu(II) addition (*ca*. 20-30% and 80% decrease in intensity respectively) with almost no change in the emission wavelength. Fluorescence intensities were recorded upon addition of increasing concentrations of metal ions and the data were analyzed using equation 3 to determine the dissociation constants (Table 3). The intensity changes upon metal addition were fitted to determine the dissociation constants (See SI). The data were fitted considering only one metal binding to the protein (using equation 3) and no other dissociation constant had to be included to reproduce the experimental data.

The dissociation constant for Fe(II) in the native enzyme is found equal to 4.4 μM. This value is close to the ones previously determined for tomato ACCO [29,48]. This value is also in the same order of magnitude as the Michaelis-Menten constant derived from kinetic measurements (Table **2**). Mutation of the aspartate ligand into coordinating aminoacids (histidine or glutamate) does not drastically affect the affinity for iron(II) (Kd of 7.1 and 8.6 μM respectively). Extending the length of the aminoacid side-chain by replacing the aspartate by a glutamate residue (D179E) induces a loss of activity although iron binding occurs with a comparable affinity. Finally, the D179A variant displays a decreased affinity for Fe(II) (Kd = 23.6 μM) in agreement with the removal of one ligand.

The affinity of the native enzyme for Cu(II) is similar to the one for Fe(II) as already observed in related 2-oxoglutarate dependent dioxygenases [55]. Mutations of the aspartate residue into histidine and alanine have a limited effect on the affinity for Cu(II) (Kd of 4.1 and 3.8 μM respectively). In contrast, the variant D179E displays lower affinity for Cu(II) with a dissociation constant of 26.5 μM.

Table 3: Metal dissociation constants determined by intrinsic fluorescence quenching (K_d expressed in μM).

	Native	D179H	D179A	D179E
Fe(II)	4.4 ± 1.2	7.1 ± 1.0	23.6 ± 4.7	8.6 ± 2.6
Cu(II)	5.5 ± 0.6	4.1 ± 0.3	3.8 ± 0.3	26.5 ± 2.6

Activity of copper-reconstituted-ACCO enzymes

We evaluated the activity of the different enzymes reconstituted with copper. The ethylene production of the native and variant enzymes in the presence of copper was first measured using standard assay conditions. The enzymes were therefore placed in the presence of the cofactors / cosubstrates at normal concentrations but Fe(II) was replaced by Cu(II). Different concentrations (ACCO, substrates/cofactors, Cu) as well as different reaction times (from 5 minutes to 1 hour) were evaluated. Ethylene production was also tested in absence of bicarbonate. In normal assay conditions, no ethylene production was observed when Fe(II) was substituted by Cu(II) in the reaction mixture using either the native or variant enzymes.

We therefore tested the copper-based ethylene production in the presence of hydrogen peroxide following our procedure reported for the model complexes [20]. ACCO (native or variant) was placed at 100-200 μM in the presence of 1 eq. of Cu(II) and 1 to 10 eq. of ACC to preform the "ACCO-Cu-ACC" ternary complex. Hydrogen peroxide (1-10 equivalents) was then injected through the septum and ethylene was measured after *ca*. 1 hour of reaction time. Different buffers and pHs were tested as well as the effect of the presence or not of bicarbonate cofactor (see experimental section for details). Traces of ethylene (< 2% yield) were detected but ethylene was also produced in the control conditions in the absence of enzymes. Therefore, no copper-reconstituted enzyme-driven ethylene production was detected in any of the tested conditions.

Inhibition studies

In the absence of copper-derived activity in normal assay conditions, we performed inhibition assays. Inhibition of native ACCO by Cu(II) with Fe(II) as the varying cofactor was measured (see SI). From Lineweaver-Burk representation of data, it can be concluded that Cu(II) is a competitive inhibitor of Fe(II). An inhibition constant, K_i = 0.8 μM, was obtained by fitting simultaneously the set of curves with equation 2 (experimental part). This inhibition constant is of same order of magnitude as the determined dissociation constant of *ca*. 4 μM (Table 3). Brunhuber *et*. *al*. have reported that several divalent metal ions (such as Co(II), Zn(II) and Mn(II)) are competitive inhibitors of ACCO *versus* Fe(II) [49]. However, the observed inhibition constants ranged from 0.5 to 50 mM and therefore Cu(II) is a much stronger inhibitor of ACCO than the previously reported metal ions. Similar relatively strong competitive inhibition of Cu(II) *versus* Fe(II) has already been reported for related enzymes [56,57]. These results suggest that Cu(II) binds to the active site and efficiently competes with Fe(II) binding.

Copper reconstitution and X-band EPR characterization

To check if ACCO was correctly folded after incorporation of Cu(II), we measured the far-UV CD spectrum before or after addition of 1-20 equivalents of $CuSO_4$. The CD spectra are highly similar to each other indicating that no major secondary structure changes occur upon copper binding (see SI).

In order to better characterize the environment of the metal ion, *cw* X-band EPR spectra of the copper-reconstituted enzymes were recorded by mixing the enzymes with 0.9 equivalent of Cu(II) (Figure 2). Spectral parameters were estimated by graphical extraction from the spectra then optimized using a fitting numerical simulation (Table 4). Longitudinal parameters $A_{//}$ and $g_{//}$ are given with a good accuracy (± 5 MHz and ± 0.005 respectively). A small rhombicity of

the g-tensor was included for a better simulation of the high-field part of the spectra. Transverse Cu hyperfine constants are not resolved and do not have a strong effect on the lineshape. However we managed to estimate a threshold for all the spectra: $A_{\perp} < 70$ MHz.

The superhyperfine interactions between the Cu(II) electronic spin and the ^{14}N nuclear spins are not well resolved in the measurements. However using the pseudomodulation technique it is possible to compute the second harmonic of the EPR signal and increase the resolution [32]. The pseudomodulation consists of an enhanced derivation of the signal. Using the digitalized experimental EPR signal, the derivative of the signal is computed using fake magnetic field modulation amplitude. Thus the noise created by the standard derivative of a digitalized signal is highly reduced. The hyperfine signal from the nitrogen atoms is therefore much more resolved and it is possible to graphically extract a similar value for all spectra of $A_N = 40$ MHz (see SI). This value was used in the simulations of the first derivative spectra. The EPR parameters for the native ACCOCu(II) enzyme are $g_{//} = 2.270$, $A_{//} = 490$ MHz, $g_1 = 2.04$, $g_2 = 2.06$. These quasi-axial parameters are consistent with a type-2 copper center coordinated by a mixture of N and O ligands in the equatorial plan [58,59]. Mutation of the aspartate ligand induces small changes of the EPR parameters (Table 4).

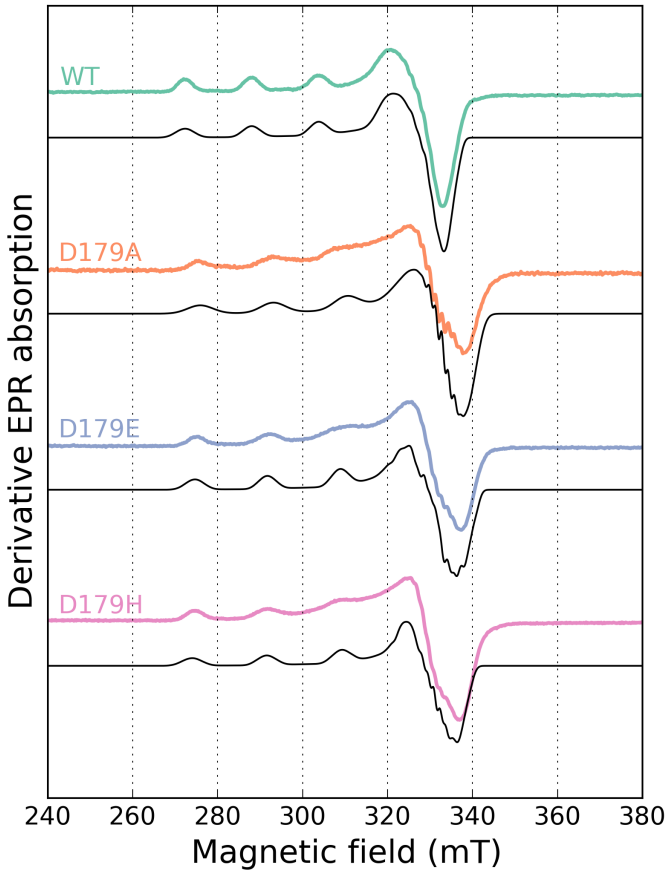

Figure 2. Experimental (color) and simulated (black) *cw* X-band EPR spectra of the Cu(II) reconstituted ACCO and D179X variants.

Table 4. Comparison of the EPR parameters for the copper-reconstituted enzymes obtained from simulation of the experimental spectra and derived from DFT calculations for the best models. The hyperfine coupling constants are expressed in MHz.

Enzyme		g_1	g_2	g_3 ($g_{//}$)	$\lvert A_1 \rvert$	$\lvert A_2 \rvert$	$\lvert A_3 \rvert$ ($\lvert A_{//} \rvert$)
Native	Exp.	2.04	2.06	2.275	<70	<70	490
	Calculated	2.068	2.105	2.280	48	48	499
D179A	Exp.	2.05	2.07	2.250	<70	<70	535
	Calculated	2.064	2.072	2.250	32	57	558
D179E	Exp.	2.03	2.08	2.260	<70	<70	530
	Calculated	2.062	2.108	2.276	51	67	535
D179H	Exp.	2.05	2.08	2.260	<70	<70	545
	Calculated*	2.053	2.094	2.246	30	52	573
Native+ACC	Exp.	2.04	2.06	2.267	<70	<70	510
	Calculated	2.055	2.086	2.230	61	66	515

* for H179 not coordinated to the copper

ESEEM spectroscopy of copper-substituted enzymes

In an attempt to better characterize the copper ligand environment, 3-pulse ESEEM data were recorded for the native enzyme and the D179H variant. The Fourier transform of the experimental time-domain data are shown in Figure 3. The spectrum of the native enzyme contains three main peaks at 0.6, 1.0 and 1.6 MHz together with a broad feature around 4.3 MHz. This is typical for the distal nitrogen from a histidine residue bound equatorially to the Cu ion. In addition, combination peaks can be clearly detected at 2.1, 2.4 and 3.2 MHz indicating that at least two histidine ligands are coordinated in the equatorial plane [60]. Given the structure known for the Fe-bound enzyme we can conclude that the Cu ion is probably equatorially bound by the two histidine residues of the facial triad residues, H177 and H234.

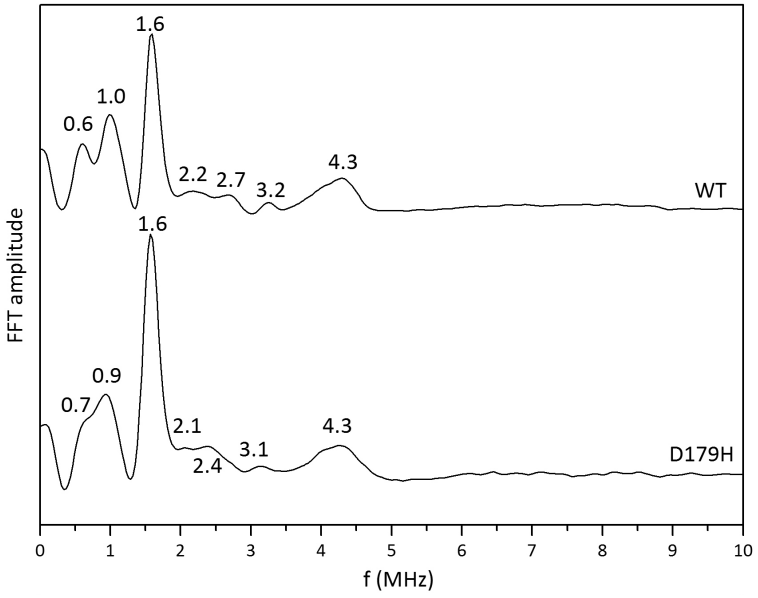

Figure 3. Fourier transform of 3-pulse ESEEM for the Cu-ACCO WT (top) and Cu-D179H mutant (bottom). Experimental conditions: B=335 mT, τ=120 ns, ν_{mw}=9.69 GHz, T 4K.

The ESEEM data for the D179H variant are very similar to the one of the native enzyme. Features are slightly broader and the two lowest frequencies slightly shifted compared to the

native enzyme's spectrum suggesting small structural reorganization for the mutant consistent with changes observed also in the *cw* EPR spectra of the two samples. The combination peaks are still observed so at least two histidine residues are bound. Even though it can be difficult to distinguish with certainty between 2 or 3 histidines bound, the amplitude of the combination peaks compared to that of the fundamental peaks are rather similar for both variant and native enzymes suggesting preferably that the number of histidines bound is the same in the D179H variant as in the native enzyme. The amplitude of the combination peaks increases with the number of bound histidine residues and becomes comparable to that of the broad feature and of the lowest fundamental frequencies for 3 or 4 His bound equatorially [60]. This is not observed here and it is therefore unlikely that the new histidine brought by the mutation is bound to the Cu ion in equatorial position.

DFT Calculations

Theoretical calculations based on Density Functional Theory (DFT) were undertaken in order to get insight into the molecular properties of the copper-reconstituted ACCO enzymes. To build up the models, several coordination environments were investigated. EPR spectra measured in Tris-H_2SO_4 buffer were found identical to the ones measured in Tris-HCl buffer. Therefore, coordination of chloride anions on the copper was not considered. We investigated several coordination possibilities including *(i)* two water molecules in the equatorial plane and *(ii)* two water molecules in the equatorial plane and one axial water molecule. Models including the coordination of hydroxide anions were also built. Finally, in the case of D179H variant, two possibilities were considered *(i)* one in which the third histidine is not bound to the copper and *(ii)* one in which the third histidine is axially bound to the copper.

Structural models for the native and variant enzymes were subjected to geometry optimizations. DFT optimized structures were used as the starting points to compute the electronic structures and magnetic properties of the models. Their EPR parameters were calculated and compared to the experimental data to select the best structural models. The resulting structures, selected as above-mentioned, are shown in Figure 4 together with selected metrical parameters. The "best" optimized structure of the native enzyme consists of a Cu(II) ion equatorially coordinated by the two histidines and two water molecules, the aspartate being bound in axial position. The structural index calculated as defined by Addison et al. is $\tau = 0.12$ indicating a slight deviation from ideally square-pyramidal geometry, in agreement with the EPR parameters [61]. Alternative models including either an additional coordinating water molecule in axial position or hydroxide ligands are presented in SI.

Mutation of aspartate 179 to glutamate (D179E) resulted in a similar structure although slightly more distorted from square-pyramidal geometry ($\tau = 0.22$). The structure of the D179A enzyme consists of a distorted square-planar Cu(II) ion with no ligand in axial position. Finally, the third histidine ligand D179H variant is predicted uncoordinated to the metal ion. The model in which this third histidine is axially coordinated is presented in SI.

The predicted EPR parameters of native and D179E, D179A, D179H "best" models are reported in Table 4. Our calculations predict axial sets of parameters, which are consistent with the simulated spectra. Additionally, low-field g-values are adequately reproduced by our calculations with computed values of 2.280 *vs*. 2.275 for native; 2.250 *vs*. 2.250 for D179A and 2.276 *vs*. 2.260 for D179E. In the case of D179H, the model with uncoordinated H179 is the one best matching the simulated data as it features an axial g-tensor with a low-field value that compares well with the experiment (2.246 *vs*. 2.260). Comparison of experimental and calculated ^{63}Cu hyperfine coupling constants (hfc) also confirms the fair agreement between theory and experiment. The tensors are predicted almost axial and the maximum hfc constants

are well reproduced by our calculations with computed values of 499 *vs*. 490 MHz for native; 558 *vs*. 535 MHz for D179A; 535 *vs*. 530 MHz for D179E and 573 *vs*. 545 MHz for D179H (uncoordinated model). The other models that were considered (including the extra water molecule, the hydroxide ligands and the coordinated H179 in the case of D179H) resulted in calculated EPR parameters that were less representative of the experimental data. In particular significant rhombicity of the g and A-tensors are predicted for the latter models, which are less consistent with the observed experimental data (see SI).

Finally, the computed SOMOs for the different models have dominant metal-based character (Cu $3dx^2$-y^2) with non-negligible contributions of the coordinating atoms of the ligands due to the covalence of the metal-ligand bonds (See SI). The Mulliken population analysis further supports that the spin density is mainly distributed over the metal and the first coordination sphere atoms since positive spin populations are found at the Cu ion, the oxygen and nitrogen centers. These latter data also provide some insight about the covalence of the Cu(II) coordination sphere. We observe an increase of the electron density at the metal site when going from the native model (spin population of 0.586) to the D179H uncoordinated one (spin population of 0.694). This suggests a decrease of the metal covalence that can be directly correlated with increased magnitude of the $A_{//}$ hyperfine coupling constants (Table 4).

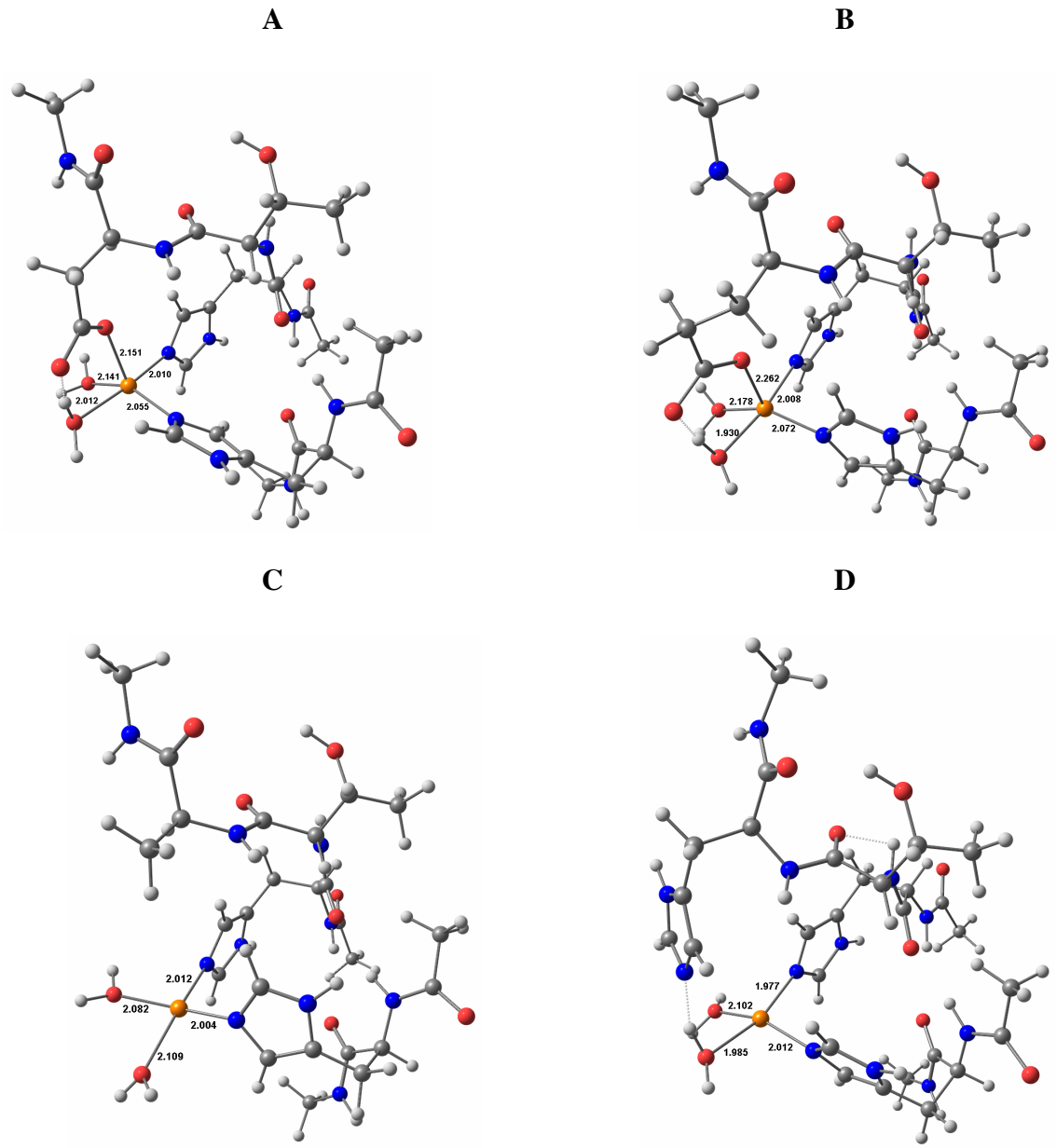

Figure 4. Structural models and selected metrical parameters for the native (**A**) and variant enzymes (**B**: D179E; **C**: D179A and **D**: D179H) obtained from DFT geometry optimizations.

ACC binding to ACCOCu(II) enzyme: EPR and DFT-calculations

In order to better understand the lack of reactivity of the copper-reconstituted enzymes, we recorded the *cw* EPR spectrum of the copper-reconstituted native ACCO in the presence of increasing amount of ACC (1-10 equivalents). ACC binding studies were conducted in two different buffers and pHs to make a parallel with the reactivity studies (either Tris-HCl pH 7.2

with 10% glycerol or MES pH 6.5 with 10% glycerol). Similar results were obtained in the different buffers. After addition of ACC, the initial spectrum is slightly modified and the signal stabilizes after 3-5 equivalents of substrate to provide the experimental spectrum displayed on Figure 5. Simulation of the main spectral features was performed as above-mentioned and the EPR parameters corresponding to the ACCO-Cu-ACC species are $g_{//}$= 2.267, $A_{//}$= 510 MHz, g_1 = 2.04 and g_2 = 2.06 (Table 4). Controls were conducted to verify that this EPR signal is not due to free copper or Cu-ACC complex in buffer solution. The parameters of the ternary ACCO-Cu-ACC complex are close to the ones obtained without bound ACC suggesting that no drastic structural changes occur around the metal ion. These quasi-axial parameters are indicative of a copper center coordinated by a mixture of N and O ligands (N_2O_2) in the equatorial plan, therefore raising the question of the bidentate coordination of ACC [58,59].

In order to get deeper insight into the ACC binding on the copper-reconstituted ACCO, structural models were constructed for the ACCO-Cu-ACC ternary complex. Several conformations and binding modes of ACC were considered (bidentate or monodentate, different coordination positions) and the resulting models were subjected to geometry optimizations. The EPR parameters of the DFT-optimized models were then computed and compared to the experimental ones. A fair agreement was observed between both sets of data when considering one peculiar ACCO-Cu-ACC model (Table 4). In this DFT-optimized model, ACC binds in a monodentate mode by an oxygen of the carboxylate function. This oxygen from ACC is bound either *trans* to H177 (displayed on Figure 5) or *trans* to H234. On the basis of the EPR parameters, it was not possible to distinguish between these two coordination positions. The other coordination modes provided parameters that were not in agreement with experimental ones and the results are displayed in SI.

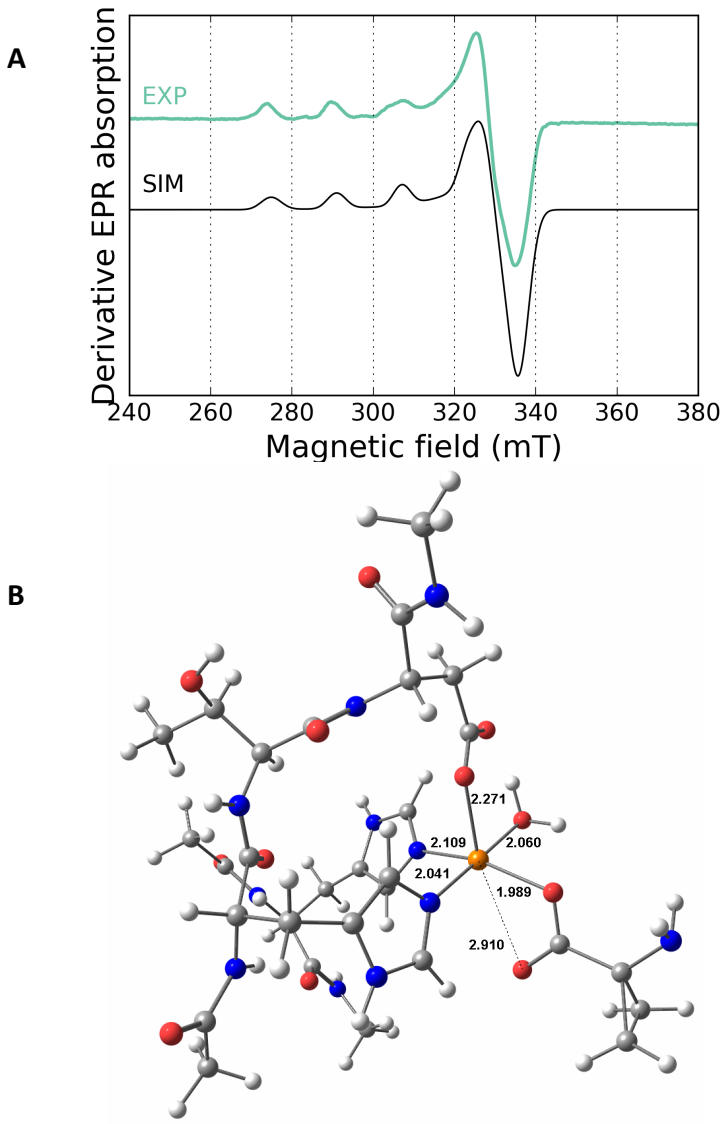

Figure 5. (A) Experimental and simulated *cw* X-band EPR spectrum of native ACCO-Cu placed in the presence of 3 equivalents of ACC in MES buffer pH 6.5 + 10% glycerol. Signals from the initial ACCOCu species can still be seen on the spectrum (B) Structural model and selected metrical parameters for the native ACCO-Cu-ACC enzyme obtained from DFT geometry optimizations.

Discussion

We have performed site-directed mutagenesis to replace the aspartate ligand of ACCO by an alanine (D179A), a histidine (D179H) or a glutamate (D179E) in order to investigate the effect of the coordination sphere on metal-binding properties and reactivity. In particular, in this work, we were interested in understanding the properties of copper-bound ACCO.

The variants were first characterized with their natural iron cofactor. Removal of the coordinating residue D179 by a non-coordinating one (alanine) induces a 4 to 5-fold decrease in iron binding affinity, as evidenced by fluorescence quenching experiments (Table 3). The other variants display dissociation constants of the same order of magnitude as the native enzyme (Kd ≈ 4 - 8 μM). All the D179 variants are inactive in the presence of their natural iron cofactor. This suggests that variation of D179 residue of ACCO, although having a minor impact on iron affinity induces significant structural and/or electronic changes at the metal center. It has to be noted that, in 2-oxoglutarate dependent oxygenases, a glutamate residue is present in 20% of the cases instead of the aspartate in the coordination sphere of the iron [62]. Here the D179E mutant is inactive. In tomato ACCO, replacement of the coordination sphere aspartate by a glutamate induced a significant loss of activity and the variant displayed only 0.1-0.2% residual activity [63]. Therefore, although the nature of the coordinating moiety is conserved (carboxylate function), extending the length of the aminoacid side-chain has a drastic effect on the activity of the iron ion, suggesting that geometrical changes may occur modifying the metal environment.

Using kinetic inhibition assays and tryptophan fluorescence quenching, we then verified that Cu(II) efficiently binds to the native and variant enzymes and competes with Fe(II) binding (Table 3). Mutations of the aspartate residue into histidine and alanine did not affect binding affinity for Cu(II) (Kd ≈ 4 μM for WT, D179H and D179A enzymes). Replacement of the aspartate by a glutamate induces a decrease in copper binding affinity (Kd ≈ 26 μM for D179E variant), supporting the fact that geometrical constrains and sterical effects may occur upon increasing the side-chain length, as observed with the iron cofactor. These results also suggest that the aspartate ligand is not essential for Cu(II) binding, since its replacement by a

non-coordinating residue does not significantly influence the dissociation constant. EPR experiments (*cw* and pulsed) and DFT-calculations indicate that, in all investigated enzymes the Cu(II) ion is equatorially bound to two histidines (H177 and H234) and two water molecules. Mutation of D179 residue into histidine did not lead to the coordination of an additional histidine in the equatorial plane. Altogether, these data are consistent with our models in which D179 residue is bound in axial position (Figure 4). The square-pyramidal coordination environment of copper(II) in ACCO is significantly different from the octahedral coordination of the native iron(II) ion. This difference can be rationalized on the basis of Jahn-Teller distortion that is very common in Cu(II) centers due to d^9 electronic configuration [64,65]. Our structural models are also consistent with data reported in the literature for the copper-reconstituted TfDA, a herbicide-degrading 2-oxoglutarate dependent enzyme [56,57,66,67]. Indeed, EPR/ESEEM experiments (including D_2O exchange and ^{2}H-ESEEM) together with XAS experiments have provided a model for the copper-binding site that contains two equatorially coordinated histidines, two equatorial water molecules and probably an additional axial water molecule. Finally, our results indicate that variations of D179 residue of ACCO induce notable geometric and electronic changes at the copper center (as probably in the case of iron) since significant differences in geometry and electron density are calculated upon replacement of the aspartate ligand.

No copper-based activity of the ACCO enzymes could be detected. To the best of our knowledge, no copper-dependent or even other metal-dependent activity has ever been evidenced in the 2-oxoglutarate dependent dioxygenase enzymes family that is highly selective for iron(II). However, the reasons for such metal selectivity remain unclear and have never been really addressed. Several reasons can be hypothesized. One could rely on the redox potential of the ACCOCu(II) centers. Indeed, we have observed, using EPR

spectroscopy and upon addition of increasing amount of ascorbate, that the Cu(II)-reconstituted ACCOs were very difficult to reduce using ascorbate, the co-substrate of ACCO in activity assays. We have previously reported that simple copper-ACC complexes (Scheme 2) were able to produce ethylene from the bound ACC moiety when reacted with hydrogen peroxide, a two electron reduced form of dioxygen [20,22,23]. For this reason, ethylene production mediated by ACCO-Cu enzymes was also evaluated using a peroxide-shunt assay. Again, no ethylene was produced under any of the conditions tested. We were therefore interested in monitoring the binding of ACC at the active site. EPR experiments coupled with DFT calculations were used to propose a model for the ACCO-Cu-ACC ternary complex. In this model, ACC is equatorially bound to the copper ion in a monodentate fashion by its carboxylate function (Figure 5). In absence of crystallographic data on substrate's binding on the natural iron(II) cofactor, ENDOR experiments have led to a model in which binding of ACC to ACCO-Fe enzyme occurs in a bidentate manner *via* its amine and carboxylate functions [15,29]. The O-atom from ACC is found to be bound *trans* to D179 and the N-atom *trans* to H177 or H234. In the present case, coordination preference of copper(II) and Jahn-Teller effect renders the position *trans* to D179 not favorable for strong ACC binding and subsequent reactivity. This is supported by the poor agreement obtained when comparing the experimental data to the theoretical EPR parameters of the DFT-optimized model constructed with bidentate coordination of ACC on the copper ion (see SI). The coordination mode of ACC on ACCO-Cu enzyme is therefore different from the one on ACCO-Fe enzyme. This coordination mode is also different from the one obtained with the low molecular weight models including the copper-based models [20,21] and probably partially accounts (amongst other factors such as redox potential values) for the lack of reactivity observed here, even in the presence of hydrogen peroxide.

Conclusion

In the present study we have characterized for the first time a copper-reconstituted native ACCO and several active-site variants using experimental and theoretical approaches. From our experimental results, it is clear that Cu(II) coordinates to the active site residues with good affinity. The proposed structural models of the copper-reconstituted enzymes consist of Cu(II) ions bound equatorially to two histidines and two water molecules. D179 in the native enzymes probably occupies an axial position on the copper ion. Although different from the Fe-coordination environment, this *N2* copper-environment is similar to that found in various model complexes. However, EPR experiments coupled with DFT-calculations indicate that binding of ACC on the metal ion probably does not occur in a bidentate mode, providing a possible explanation for the lack of reactivity of copper-reconstituted ACCO, even when using peroxide shunt reaction. Taken together, these results offer valuable insights into the molecular basis of the often unintended effects that metal and ligand variations have in this enzyme family and that are too often unexplored, hampering an in depth understanding of structure-function relationships. These insights may therefore be of interest for everyone who intends to harness metal enzymes with new functions by metal and binding motif variations.

Aknowledgements

This work has been carried out thanks to the support of the A*MIDEX project (n° ANR-11-IDEX-0001-02) funded by the « Investissements d'Avenir » French Government program, managed by the French National Research Agency (ANR). This work was also in part supported by a young researcher's grant from the ANR (ANR-09-JCJC-0080), the French Infrastructure for Integrated Structural Biology (FRISBI) funded by the « Investissements d'Avenir » French Government program, managed by the French National Research Agency

(ANR-10-INSB-05-01) and the TGE "Réseau National de RPE interdisciplinaire", FR-CNRS 3443. Finally The EU-COST Network (CM1305) on spin state reactivity is acknowledged for support.

References

[1] A.B. Bleecker, H. Kende, Ethylene: a gaseous signal molecule in plants, Annu. Rev. Cell Dev. Biol. 16 (2000) 1–18. doi:10.1146/annurev.cellbio.16.1.1.

[2] D.O. Adams, S.F. Yang, Ethylene biosynthesis: Identification of 1-aminocyclopropane-1-carboxylic acid as an intermediate in the conversion of methionine to ethylene, Proc. Natl. Acad. Sci. U.S.a. 76 (1979) 170–174. doi:10.1073/pnas.76.1.170.

[3] L.J. Murphy, K.N. Robertson, S.G. Harroun, C.L. Brosseau, U. Werner-Zwanziger, J. Moilanen, et al., A Simple Complex on the Verge of Breakdown: Isolation of the Elusive Cyanoformate Ion, Science. 344 (2014) 75–78. doi:10.1126/science.1250808.

[4] M. Costas, M.P. Mehn, M.P. Jensen, L. Que, Dioxygen Activation at Mononuclear Nonheme Iron Active Sites: Enzymes, Models, and Intermediates, Chem. Rev. 104 (2004) 939–986. doi:10.1021/cr020628n.

[5] A.J. Simaan, M. Réglier, ACC Oxidase and Ethylene Biosynthesis in Plants, in: R.P. Hausinger, C.J. Schofield (Eds.), 2-Oxoglutarate-Dependent Oxygenases, Royal Society of Chemistry, Cambridge, 2015: p. 425.

[6] S.F. Yang, N.E. Hoffman, Ethylene Biosynthesis and its Regulation in Higher Plants, Annu. Rev. Plant. Physiol. 35 (1984) 155–189. doi:10.1146/annurev.pp.35.060184.001103.

[7] J.G. Dong, J.C. Fernández-Maculet, S.F. Yang, Purification and characterization of 1-aminocyclopropane-1-carboxylate oxidase from apple fruit, Proc. Natl. Acad. Sci. U.S.a. 89 (1992) 9789–9793. doi:10.1073/pnas.89.20.9789.

[8] Z. Zhang, J.-S. Ren, I.J. Clifton, C.J. Schofield, Crystal Structure and Mechanistic Implications of 1-Aminocyclopropane-1-Carboxylic Acid Oxidase—The Ethylene-Forming Enzyme, Chem. Biol. 11 (2004) 1383–1394. doi:10.1016/j.chembiol.2004.08.012.

[9] J. Zhou, A.M. Rocklin, J.D. Lipscomb, L. Que, E.I. Solomon, Spectroscopic Studies of 1-Aminocyclopropane-1-carboxylic Acid Oxidase: Molecular Mechanism and CO_2 Activation in the Biosynthesis of Ethylene, J. Am. Chem. Soc. 124 (2002) 4602–4609. doi:10.1021/ja017250f.

[10] R.P. Hausinger, Fe(II)/α-Ketoglutarate-Dependent Hydroxylases and Related Enzymes, Critical Reviews in Biochemistry and Molecular Biology. 39 (2004) 21–68. doi:10.1080/10409230490440541.

[11] I.J. Clifton, M.A. McDonough, D. Ehrismann, N.J. Kershaw, N. Granatino, C.J. Schofield, Structural studies on 2-oxoglutarate oxygenases and related double-stranded β-helix fold proteins, J. Inorg. Biochem. 100 (2006) 644–669. doi:10.1016/j.jinorgbio.2006.01.024.

[12] R.P. Hausinger, C.J. Schofield, eds., 2-Oxoglutarate-Dependent Oxygenases, Royal Society of Chemistry, Cambridge, 2015. doi:10.1039/9781782621959.

[13] M.C. Pirrung, Ethylene Biosynthesis from 1-Aminocyclopropanecarboxylic Acid, Acc. Chem. Res. 32 (1999) 711–718. doi:10.1021/ar960003.

[14] A.M. Rocklin, D.L. Tierney, V. Kofman, N.M. Brunhuber, B.M. Hoffman, R.E. Christoffersen, et al., Role of the nonheme Fe(II) center in the biosynthesis of the plant hormone ethylene, Proc. Natl. Acad. Sci. U.S.a. 96 (1999) 7905–7909.

[15] D.L. Tierney, A.M. Rocklin, J.D. Lipscomb, L. Que, B.M. Hoffman, ENDOR Studies of the Ligation and Structure of the Non-Heme Iron Site in ACC Oxidase, J. Am. Chem. Soc. 127 (2005) 7005–7013. doi:10.1021/ja0500862.

[16] A.M. Rocklin, K. Kato, H.-W. Liu, L. Que, J.D. Lipscomb, Mechanistic studies of 1-

aminocyclopropane-1-carboxylic acid oxidase: single turnover reaction, J Biol Inorg Chem. 9 (2004) 171–182. doi:10.1007/s00775-003-0510-3.

[17] L.M. Mirica, J.P. Klinman, The nature of O2 activation by the ethylene-forming enzyme 1-aminocyclopropane-1-carboxylic acid oxidase, Proc. Natl. Acad. Sci. U.S.a. 105 (2008) 1814–1819. doi:10.1073/pnas.0711626105.

[18] Y. Roux, W. Ghattas, F. Avenier, R. Guillot, A.J. Simaan, J.P. Mahy, Synthesis and characterization of [Fe(BPMEN)ACC]SbF 6: a structural and functional mimic of ACC-oxidase, Dalton Trans. 44 (2015) 5966–5968. doi:10.1039/C5DT00347D.

[19] M. Sallmann, F. Oldenburg, B. Braun, M. Réglier, A.J. Simaan, C. Limberg, A Structural and Functional Model for the 1-Aminocyclopropane-1-carboxylic Acid Oxidase, Angew. Chem. Int. Ed. 54 (2015) 12325–12328. doi:10.1002/anie.201502529.

[20] W. Ghattas, C. Gaudin, M. Giorgi, A. Rockenbauer, A.J. Simaan, M. Réglier, ACC-Oxidase like activity of a copper (II)–ACC complex in the presence of hydrogen peroxide. Detection of a reaction intermediate at low temperature, Chem. Commun. (2006) 1027–1029. doi:10.1039/B515374C.

[21] W. Ghattas, M. Giorgi, Y. Mekmouche, T. Tanaka, A. Rockenbauer, M. Réglier, et al., Identification of a Copper(I) Intermediate in the Conversion of 1-Aminocyclopropane Carboxylic Acid (ACC) into Ethylene by Cu(II)–ACC Complexes and Hydrogen Peroxide, Inorg. Chem. 47 (2008) 4627–4638. doi:10.1021/ic702303g.

[22] W. Ghattas, M. Giorgi, C. Gaudin, A. Rockenbauer, M. Réglier, A.J. Simaan, Characterization of Cu(II)-ACC complexes and conversion of the bound ACC into ethylene in the presence of hydrogen peroxide. detection of a brown intermediate at low temperature, Bioinorg Chem Appl. 2007 (2007) 43424–9. doi:10.1155/2007/43424.

[23] J.S. Pap, N. El Bakkali-Taheri, A. Fadel, S. Góger, D. Bogáth, M. Molnár, et al., Oxidative Degradation of Amino Acids and Aminophosphonic Acids by 2,2′-Bipyridine Complexes of Copper(II), Eur. J. Inorg. Chem. 2014 (2014) 2829–2838. doi:10.1002/ejic.201400133.

[24] D. Lakk-Bogáth, M. Molnár, G. Speier, M. Giorgi, J. Kaizer, Ligand-dependent oxidation of copper bound α-amino-isobutyric acid as 1-aminocyclopropane-1-carboxylic acid oxidase mimics, Polyhedron. 98 (2015) 12–17. doi:10.1016/j.poly.2015.05.043.

[25] S. Hong, S.M. Huber, L. Gagliardi, C.C. Cramer, W.B. Tolman, Copper(I)-alpha-ketocarboxylate complexes: characterization and O2 reactions that yield copper-oxygen intermediates capable of hydroxylating arenes, J. Am. Chem. Soc. 129 (2007) 14190–14192. doi:10.1021/ja0760426.

[26] A.K. Gupta, W.B. Tolman, Copper/alpha-ketocarboxylate chemistry with supporting peralkylated diamines: reactivity of copper(I) complexes and dicopper-oxygen intermediates, Inorg. Chem. 49 (2010) 3531–3539. doi:10.1021/ic100032n.

[27] E.I. Solomon, D.E. Heppner, E.M. Johnston, J.W. Ginsbach, J. Cirera, M. Qayyum, et al., Copper active sites in biology, Chem. Rev. 114 (2014) 3659–3853. doi:10.1021/cr400327t.

[28] E.A. Lewis, W.B. Tolman, Reactivity of Dioxygen–Copper Systems, Chem. Rev. 104 (2004) 1047–1076. doi:10.1021/cr020633r.

[29] L. Brisson, N. Bakkali-Taheri, M. Giorgi, A. Fadel, J. Kaizer, M. Réglier, et al., 1-Aminocyclopropane-1-carboxylic acid oxidase: insight into cofactor binding from experimental and theoretical studies, J Biol Inorg Chem. 17 (2012) 939–949. doi:10.1007/s00775-012-0910-3.

[30] A. Cornish-Bowden, A simple graphical method for determining the inhibition constants of mixed, uncompetitive and non-competitive inhibitors, Biochem. J. 137 (1974) 143–144.
[31] S. Stoll, A. Schweiger, EasySpin, a comprehensive software package for spectral simulation and analysis in EPR, J. Magn. Reson. 178 (2006) 42–55. doi:10.1016/j.jmr.2005.08.013.
[32] J.S. Hyde, M. Pasenkiewicz-Gierula, A. Jesmanowicz, W.E. Antholine, Pseudo field modulation in EPR spectroscopy, Appl Magn Reson. 1 (1990) 483–496. doi:10.1007/BF03166028.
[33] W.B. Mims, Elimination of the dead-time artifact in electron spin-echo envelope spectra, J Magn Reson. 59 (1984) 291–306. doi:10.1016/0022-2364(84)90174-4.
[34] F. Neese, The ORCA program system, WIREs Comput Mol Sci. 2 (2011) 73–78. doi:10.1002/wcms.81.
[35] J. Perdew, Density-functional approximation for the correlation energy of the inhomogeneous electron gas, Phys. Rev., B Condens. Matter. 33 (1986) 8822–8824.
[36] J. Perdew, Erratum: Density-functional approximation for the correlation energy of the inhomogeneous electron gas, Phys. Rev., B Condens. Matter. 34 (1986) 7406–7406.
[37] A. Becke, Density-functional exchange-energy approximation with correct asymptotic behavior, Phys. Rev., A. 38 (1988) 3098–3100. doi:10.1103/PhysRevA.38.3098.
[38] A. Schäfer, C. Huber, R. Ahlrichs, Fully optimized contracted Gaussian basis sets of triple zeta valence quality for atoms Li to Kr, The Journal of Chemical Physics. 100 (1994) 5829–5835. doi:10.1063/1.467146.
[39] F. Neese, An improvement of the resolution of the identity approximation for the formation of the Coulomb matrix, J Comput Chem. 24 (2003) 1740–1747. doi:10.1002/jcc.10318.
[40] F. Weigend, Accurate Coulomb-fitting basis sets for H to Rn, Physical Chemistry Chemical Physics. 8 (2006) 1057–1065. doi:10.1039/B515623H.
[41] F. Neese, Prediction of electron paramagnetic resonance g values using coupled perturbed Hartree–Fock and Kohn–Sham theory, The Journal of Chemical Physics. 115 (2001) 11080. doi:10.1063/1.1419058.
[42] S. Koseki, M.W. Schmidt, M.S. Gordon, MCSCF/6-31G(d,p) calculations of one-electron spin-orbit coupling constants in diatomic molecules, J. Phys. Chem. 96 (1992) 10768–10772. doi:10.1021/j100205a033.
[43] S. Koseki, M.S. Gordon, M.W. Schmidt, N. Matsunaga, Main Group Effective Nuclear Charges for Spin-Orbit Calculations, J. Phys. Chem. 99 (1995) 12764–12772. doi:10.1021/j100034a013.
[44] F. Neese, Metal and ligand hyperfine couplings in transition metal complexes: The effect of spin–orbit coupling as studied by coupled perturbed Kohn–Sham theory, The Journal of Chemical Physics. 118 (2003) 3939–3948. doi:10.1063/1.1540619.
[45] V. BARONE, Structure, Magnetic Properties and Reactivities of Open-Shell Species From Density Functional and Self-Consistent Hybrid Methods, in: Recent Advances in Density Functional Methods, WORLD SCIENTIFIC, 2011: pp. 287–334. doi:10.1142/9789812830586_0008.
[46] D.A. Pantazis, X.-Y. Chen, C.R. Landis, F. Neese, All-Electron Scalar Relativistic Basis Sets for Third-Row Transition Metal Atoms, J. Chem. Theory Comput. 4 (2008) 908–919. doi:10.1021/ct800047t.
[47] D.A. Pantazis, F. Neese, All-Electron Scalar Relativistic Basis Sets for the Lanthanides, J. Chem. Theory Comput. 5 (2009) 2229–2238. doi:10.1021/ct900090f.

[48] J.S. Thrower, R. Blalock, J.P. Klinman, Steady-State Kinetics of Substrate Binding and Iron Release in Tomato ACC Oxidase, Biochemistry. 40 (2001) 9717–9724. doi:10.1021/bi010329c.
[49] N.M.W. Brunhuber, J.L. Mort, R.E. Christoffersen, N.O. Reich, Steady-State Kinetic Mechanism of Recombinant Avocado ACC Oxidase: Initial Velocity and Inhibitor Studies †, Biochemistry. 39 (2000) 10730–10738. doi:10.1021/bi0000162.
[50] E. Dupille, C. Rombaldi, J.M. Lelièvre, J.C. Cleyet-Marel, J.C. Pech, A. Latché, Purification, properties and partial amino-acid sequence of 1-aminocyclopropane-1-carboxylic acid oxidase from apple fruits, Planta. 190 (1993) 65–70.
[51] J.C. Dunning Hotopp, T.A. Auchtung, D.A. Hogan, R.P. Hausinger, Intrinsic tryptophan fluorescence as a probe of metal and alpha-ketoglutarate binding to TfdA, a mononuclear non-heme iron dioxygenase, J. Inorg. Biochem. 93 (2003) 66–70.
[52] J.R. Albani, Structure and dynamics of macromolecules: absorption and fluorescence studies, 2011. doi:10.1016/b978-044451449-3/50008-3.
[53] S.S. Lehrer, Fluorescence and absorption studies of the binding of copper and iron to transferrin, J. Biol. Chem. 244 (1969) 3613–3617.
[54] W. Horrocks, [21] Luminescence spectroscopy, Methods in Enzymology. 226 (1993) 495–538. doi:10.1016/0076-6879(93)26023-3.
[55] J.C. Dunning Hotopp, T.A. Auchtung, D.A. Hogan, R.P. Hausinger, Intrinsic tryptophan fluorescence as a probe of metal and alpha-ketoglutarate binding to TfdA, a mononuclear non-heme iron dioxygenase, J. Inorg. Biochem. 93 (2003) 66–70. doi:10.1016/S0162-0134(02)00436-1.
[56] E.L. Hegg, A.K. Whiting, R.E. Saari, J. McCracken, R.P. Hausinger, L. Que, Herbicide-Degrading α-Keto Acid-Dependent Enzyme TfdA: Metal Coordination Environment and Mechanistic Insights †, Biochemistry. 38 (1999) 16714–16726. doi:10.1021/bi991796l.
[57] D.A. Hogan, S.R. Smith, E.A. Saari, J. McCracken, R.P. Hausinger, Site-directed Mutagenesis of 2,4-Dichlorophenoxyacetic Acid/α-Ketoglutarate Dioxygenase IDENTIFICATION OF RESIDUES INVOLVED IN METALLOCENTER FORMATION AND SUBSTRATE BINDING, J. Biol. Chem. 275 (2000) 12400–12409. doi:10.1074/jbc.275.17.12400.
[58] J. Peisach, W.E. Blumberg, Structural implications derived from the analysis of electron paramagnetic resonance spectra of natural and artificial copper proteins, Arch. Biochem Biophys. 165 (1974) 691–708.
[59] U. Sakaguchi, A.W. Addison, Spectroscopic and redox studies of some copper(II) complexes with biomimetic donor atoms: implications for protein copper centres, J. Chem. Soc., Dalton Trans. (1979) 600–9. doi:10.1039/dt9790000600.
[60] J. McCracken, S. Pember, S.J. Benkovic, J.J. Villafranca, R.J. Miller, J. Peisach, Electron spin-echo studies of the copper binding site in phenylalanine hydroxylase from Chromobacterium violaceum, J. Am. Chem. Soc. 110 (1988) 1069–1074. doi:10.1021/ja00212a012.
[61] A.W. Addison, T.N. Rao, J. Reedijk, J. van Rijn, G.C. Verschoor, Synthesis, structure, and spectroscopic properties of copper(II) compounds containing nitrogen?sulphur donor ligands; the crystal and molecular structure of aqua[1,7-bis(N-methylbenzimidazol-2?-yl)-2,6-dithiaheptane]copper(II) perchlorate, J. Chem. Soc., Dalton Trans. (1984) 1349–8. doi:10.1039/dt9840001349.
[62] W.S. Aik, R. Chowdhury, I.J. Clifton, R.J. Hopkinson, T. Leissing, M.A. McDonough, et al., Introduction to Structural Studies on 2-Oxoglutarate-Dependent Oxygenases and Related Enzymes, in: C.J. Schofield, R.P. Hausinger (Eds.), 2-Oxoglutarate-Dependent Oxygenases, Royal Society of Chemistry, Cambridge, 2015:

pp. 59–94. doi:10.1039/9781782621959-00059.
[63] Z. Zhang, J.N. Barlow, J.E. Baldwin, C.J. Schofield, Metal-Catalyzed Oxidation and Mutagenesis Studies on the Iron(II) Binding Site of 1-Aminocyclopropane-1-carboxylate Oxidase, Biochemistry. 36 (1997) 15999–16007. doi:10.1021/bi971823c.
[64] M.V. Veidis, G.H. Schreiber, T.E. Gough, G.J. Palenik, Jahn-Teller distortions in octahedral copper(II) complexes, J. Am. Chem. Soc. 91 (1969) 1859–1860. doi:10.1021/ja01035a051.
[65] I.B. Bersuker, Modern Aspects of the Jahn–Teller Effect Theory and Applications To Molecular Problems, Chem. Rev. 101 (2001) 1067–1114. doi:10.1021/cr0004411.
[66] A.K. Whiting, L. Que, R.E. Saari, R.P. Hausinger, M.A. Fredrick, J. McCracken, Metal Coordination Environment of a Cu(II)-Substituted α-Keto Acid-Dependent Dioxygenase That Degrades the Herbicide 2,4-D, J. Am. Chem. Soc. 119 (1997) 3413–3414. doi:10.1021/ja964449x.
[67] N.J. Cosper, C.M.V.S.X. lhandske, R.E. Saari, R.P. Hausinger, R.A. Scott, X-ray absorption spectroscopic analysis of Fe(II) and Cu(II) forms of a herbicide-degrading α-ketoglutarate dioxygenase, J Biol Inorg Chem. 4 (1999) 122–129. doi:10.1007/s007750050295.